JOURNAL OF COMPUTATIONAL PHYSICS 49, 276–297 (1983)

# An Open Boundary Condition for Incompressible Stratified Flows

T. Y. HAN, J. C. S. MENG, AND G. E. INNIS

*Science Applications, Inc., La Jolla, California 92038*

Received March 23, 1982; revised June 29, 1982

Orlanski's open boundary condition (*J. Comput. Phys.* **21** (1976), 251) with a simple finite difference representation has been tested for laminar wakes in a nonstratified fluid and for internal wave problems in a linearly stratified flow. No artificial damping or filtering is applied to minimize high-frequency errors. Three test calculations, which are all linear flow problems, are carried out and compared with the exact solutions to demonstrate the accuracy of the open boundary condition. The performance of the open boundary condition is remarkably good. The test results also confirm that this type of boundary condition, which was originally designed by Orlanski primarily for equations which are hyperbolic in nature, also performs well for parabolic problems. Attention is needed, however, on implementing an open boundary condition for the pressure equation, especially when the flow dictates that the pressure field is strongly coupled with the velocity field.

## 1. INTRODUCTION

As more sophisticated computational fluid mechanics models are developed, the problem of formulating an accurate boundary condition is becoming an interesting subject in itself. The difficulty in prescribing the boundary condition for a finite domain calculation arises mainly from the lack of fluid dynamic information outside of the computational domain. To overcome this difficulty, the tendency has been to use a larger computational domain than that dictated by the nature of the flow. Due to computer memory limitation and, hence, cost limitation, however, the domain cannot be increased indefinitely. An open-wall boundary has to be formulated which allows flow generated in the main domain of interest to pass through the boundaries without generating any significant wave reflection and, hence, without aberrating the interior solution.

Various methods, such as simple extrapolation or viscous damping near the open boundary, have been developed by many authors. It was found that none of these methods is perfect in reducing numerical reflections at the boundaries to a negligible order. A more accurate and practical formulation was given by Orlanski [1]. He used the Sommerfeld radiation condition to prescribe an open-wall boundary condition. The local wave speed at the boundary was evaluated from the neighboring grid points through the leapfrog finite difference approximation of the Sommerfeld radiation condition. He used two model problems, i.e., the collapse of a mixed region in a



0021-9991/83/020276-22$03.00/0

stratified fluid and the spatially growing Kelvin–Helmholtz instability, to demonstrate the applicability of his open-wall boundary condition.

A different finite-difference representation of Orlanski's open boundary condition was applied to study the free surface waves induced by ship motion [2]. The effectiveness of the radiation condition was well demonstrated via two linear calculations, one with a large domain and the other with a smaller domain. Recently, a simplified version of Orlanski's method was implemented by Camerlengo and O'Brien [3] to simulate the outflow of Rossby and Kelvin waves from a computational domain with open boundaries. In this modified version, the local wave speed close to the boundary was evaluated according to Orlanski's method with the exception of the following differences: if the local phase speed was pointing outward, an outflow boundary condition via a simple extrapolation was specified; on the other hand, if the local phase speed was pointing inward, an inflow boundary condition was specified.

Special care is necessary to implement an open-wall boundary condition when velocity and density are solved directly as primitive variables. Pressure in this case is directly obtained through iteration of the Poisson equation. To preserve numerical stability, special attention must be given in prescribing the open boundary condition for pressure. Unfortunately, no previous study has addressed the radiation boundary condition for the pressure equation applicable in an incompressible fluid. Instead, Orlanski formulated the boundary condition for two-dimensional problems in terms of the stream function and vorticity so that the pressure does not appear explicitly in the equation. As for the test problems of Chan [2] or Camerlengo and O'Brien [3], the pressure is constant along the free surface. For the present numerical approach solving primitive variables, especially for three-dimensional flows, however, boundary conditions for both the velocity and pressure are needed. Knowing that the pressure and the velocity field are strongly coupled through the incompressibility condition, the phase speeds for the velocity and pressure near the boundary may not be independently specified for the open boundary condition. This problem is not fully addressed in this paper. In the present method, the velocity and the pressure at the boundary, on a variable mesh, are formulated according to Orlanski's method but with a different finite-difference representation. To preserve the numerical stability, a finite-difference representation, forward in time and upwind in space, is applied in an explicit form for the velocity and in an implicit form for pressure.

Three test calculations have been carried out to demonstrate the applicability of the implemented open boundary condition. They are (i) laminar nonstratified wake of a towed axisymmetric body, (ii) laminar nonstratified wake of a self-propelled axisymmetric body, and (iii) collapse of a well-mixed region in a linear stratified fluid. These calculations were carried out in a linear regime in order to enable a direct comparison of the calculated results with the exact solutions. The performance of the present version of the open-wall boundary condition is remarkably good in comparison with a free-slip boundary condition (or symmetry boundary condition). It is found that by using the open boundary condition formulated here the computational cost is reduced by a factor of two without sacrificing the accuracy of the solution in the main interior region of the computational domain.

## 2. Governing Equations and Numerical Scheme

We consider the three-dimensional steady motion of a density-stratified fluid. Using rectangular Cartesian coordinates $(x, y, z)$, we define $x$ as the axial mean flow direction, $y$ and $z$ as the horizontal and vertical directions, respectively, and $(U_0 + u, v, w)$ as the corresponding components of the fluid velocity. We have decomposed the axial velocity component into a mean (constant) value $U_0$ and a deviation of $u$. The equilibrium density $\rho_0$ is assumed to be a function of the vertical coordinate $z$ only. Neglecting streamwise diffusion and applying the Boussinesq approximation, we obtain the following equations of motion for an incompressible fluid:

$$U_0 \frac{\partial u}{\partial x} = -\frac{\partial uv}{\partial y} - \frac{\partial uw}{\partial z} + \nu\left(\frac{\partial^2 u}{\partial y^2} + \frac{\partial^2 u}{\partial z^2}\right), \tag{2.1}$$

$$\frac{\partial (U_0 + u)v}{\partial x} = -\frac{1}{\rho_0}\frac{\partial p}{\partial y} - \frac{\partial v^2}{\partial y} - \frac{\partial vw}{\partial z} + \nu\left(\frac{\partial^2 v}{\partial y^2} + \frac{\partial^2 v}{\partial z^2}\right), \tag{2.2}$$

$$\frac{\partial (U_0 + u)w}{\partial x} = -\frac{1}{\rho_0}\frac{\partial p}{\partial z} - \frac{\partial vw}{\partial y} - \frac{\partial w^2}{\partial z} - \frac{\rho' g}{\rho_0} + \nu\left(\frac{\partial^2 w}{\partial y^2} + \frac{\partial^2 w}{\partial z^2}\right), \tag{2.3}$$

$$\frac{\partial (U_0 + u)\rho'}{\partial x} = -\frac{\partial v\rho'}{\partial y} - \frac{\partial w\rho'}{\partial z} - w\frac{d\rho_0}{dz}, \tag{2.4}$$

$$\frac{\partial u}{\partial x} + \frac{\partial v}{\partial y} + \frac{\partial w}{\partial z} = 0, \tag{2.5}$$

where $p$ is the pressure, $\rho'$ is the density deviation from the ambient state $\rho_0(z)$, $g$ is the gravitational constant, and $\nu$ is the kinematic viscosity of the fluid. It should be mentioned that the apparent simplicity of Eq. (2.1) results from the linearization of $\partial(U_0 + u)^2/\partial x$ and the neglect of the axial pressure gradient. Therefore, these model equations are suitable for calculations of laminar wakes in a stratified fluid.

By setting $u = 0$, $U_0 = 1$, and $x = t$, where $t$ is time, Eqs. (2.2)–(2.5) are converted into a system of equations suitable for calculation of two-dimensional unsteady flows. Given a consistent set of information on an initial $y - z$ plane, Eqs. (2.1)–(2.5) can be used to "march" in the positive $x$-direction to obtain the downstream flow field, since these equations constitute a perabolic system. Thus, the numerical integration with respect to $x$, in this case, is equivalent to a time integration in a two-dimensional time-dependent problem.

The finite-difference formulation of the above equations is similar to the scheme used by Chan [4], except for a difference in the order of numerical accuracy. Chan used an explicit two-level time integration scheme with a second-order Taylor series expansion in the marching direction, while in this paper we have retained a third-order accuracy in the marching direction. Centered differencing is used in all space

derivatives. Marching of any variable $\phi$ is obtained via a Taylor series expansion in the $x$-direction, i.e.,

$$\phi^{n+1} = \phi^n + \left(\frac{\partial \phi}{\partial x}\right)^n \Delta x + \left(\frac{\partial^2 \phi}{\partial x^2}\right)^n \frac{\Delta x^2}{2} + \left(\frac{\partial^3 \phi}{\partial x^3}\right)^n \frac{\Delta x^3}{6} + O(\Delta x^4). \tag{2.6}$$

For the calculation of two-dimensional unsteady flows, $x$ is replaced by time $t$ and the superscripts "$n+1$" and "$n$" denote the time levels. The first-order derivatives $(\partial\phi/\partial x)^n$ are obtained directly from Eqs. (2.1)–(2.4). For the second- and third-order derivatives, the right-hand side of Eqs. (2.1)–(2.4) are differentiated with respect to $x$ and a conservative flux-form differencing is applied.

The corresponding pressure field is obtained by a modified MAC method [5]. Let $\tilde{v}$ and $\tilde{w}$ denote all the terms in the Taylor series expansion for $v$ and $w$ excluding the pressure terms, so that we have

$$(U_0 + u)v^{n+1} = (U_0 + u)\tilde{v}^n - \left.\frac{\partial p}{\partial y}\right|^{n+1} \Delta x - \left.\frac{\partial^2 p}{\partial x\, \partial y}\right|^n \frac{\Delta x^2}{2}, \tag{2.7}$$

$$(U_0 + u)w^{n+1} = (U_0 + u)\tilde{w}^n - \left.\frac{\partial p}{\partial z}\right|^{n+1} \Delta x - \left.\frac{\partial^2 p}{dx\, \partial z}\right|^n \frac{\Delta x^2}{2}. \tag{2.8}$$

Substituting these expressions into the incompressibility condition, Eq. (2.5), we obtain a Poisson equation for pressure

$$\frac{\partial}{\partial y}\left(\frac{1}{(U_0+u)}\frac{\partial p}{\partial y}\right)^{n+1} + \frac{\partial}{\partial z}\left(\frac{1}{(U_0+u)}\frac{\partial p}{\partial z}\right)^{n+1}$$
$$= \frac{4}{5\Delta x}\left(\frac{\partial u}{\partial x} + \frac{\partial \tilde{v}}{\partial y} + \frac{\partial \tilde{w}}{\partial z}\right)^n + \frac{1}{5}\left[\frac{\partial}{\partial y}\left(\frac{1}{(U_0+u)}\frac{\partial p}{\partial y}\right)^{n-1} + \frac{\partial}{\partial z}\left(\frac{1}{(U_0+u)}\frac{\partial p}{\partial z}\right)^{n-1}\right]. \tag{2.9}$$

Equation (2.9) is solved using the method of successive overrelaxation (SOR).

The above numerical scheme is stable and accurate to $(\Delta x)^2$ so long as the marching increment satisfies the Courant–Friedrichs–Lewy condition. The entire system of equations is formulated on a staggered variable mesh. The mesh stretching is carefully designed to prevent unrealistic wave reflections for a linearly stratified fluid. Details of this variable mesh are relegated to Appendix A.

## 3. Open Boundary Conditions

For the study here, we are primarily concerned with internal wave phenomena for density-stratified flows which are hyperbolic in nature. The internal waves generated in the interior of the domain propagate and eventually leave the flow system. So far,

the most accurate boundary condition for a hyperbolic system is based on a Sommerfeld radiation condition at the boundary,

$$\partial\phi/\partial t + c(\partial\phi/\partial y) = 0, \tag{3.1}$$

where $\phi$ is any flow variable and $c$ is the local phase speed of the waves. The variable $t$ may be replaced with $x$ for a three-dimensional steady-state parabolic problem. Depending upon the finite-difference representation in prescribing open boundary conditions, there are several methods to implement Eq. (3.1).

3.1 *Original Orlanski Method* [1]

Consider the simplest case of a monochromatic wave propagating through the right vertical boundary. Using a leapfrog finite-difference representation of Eq. (3.1) for any variable, we have

$$(\phi_k^{n+1} - \phi_k^{n-1})/2\Delta t = -(c/\Delta y)[\tfrac{1}{2}(\phi_k^{n+1} + \phi_k^{n-1}) - \phi_{k-1}^n], \tag{3.2}$$

where the index $k$ denotes a point at a boundary. The phase speed is numerically evaluated at the closest interior points from Eq. (3.2),

$$c = -\frac{(\phi_{k-1}^n - \phi_{k-1}^{n-2})}{(\phi_{k-1}^n + \phi_{k-1}^{n-2} - 2\phi_{k-2}^{n-1})}\frac{\Delta y}{\Delta t}. \tag{3.3}$$

Given a phase speed $c$, the boundary condition can be obtained from Eq. (3.2) as

$$\phi_k^{n+1} = \frac{(1 - (\Delta t/\Delta y)c)}{(1 + (\Delta t/\Delta y)c)}\phi_k^{n-1} + \frac{(2(\Delta t/\Delta y)c)}{(1 + (\Delta t/\Delta y)c)}\phi_{k-1}^n. \tag{3.4}$$

In other words, the boundary value is extrapolated from the values of $\phi$ near the boundary at previous time levels and is also a function of the phase speed $c$. For the special case $c = \Delta y/\Delta t$, this method gives the exact solution of Eq. (3.1), i.e.,

$$\phi_k^{n+1} = \phi_{k-1}^n, \tag{3.5}$$

and we may regard this as a limiting outflow condition. Conversely, in the limit of $c = 0$, we have

$$\phi_k^{n+1} = \phi_k^{n-1} \qquad \text{or a fixed } \phi \text{ boundary}, \tag{3.6}$$

i.e., no information comes from the interior solution, so we may regard this as an inflow condition, and $\phi$ can be prescribed from the previous time step or as a fixed-value boundary condition.

Since Orlanski's open boundary condition does not allow information to come from outside to inside the domain, only the outward phase speed ($c \geqslant 0$) is useful for prescribing the boundary condition. The phase speed which was evaluated from

Eq. (3.3), however, cannot be greater than the maximum speed $\Delta y/\Delta t$ from a numerical stability point of view. The final form for the phase speed, then, is

$$\begin{aligned} c &= 0, && \text{if} \quad c \leqslant 0, \\ &= \Delta y/\Delta t, && \text{if} \quad c \geqslant \Delta y/\Delta t, \\ &= -\frac{\partial\phi/\partial t}{\partial\phi/\partial y} && \text{if} \quad 0 < c < \Delta y/\Delta t. \end{aligned} \tag{3.7}$$

As a result, this boundary condition does not depend upon the global quantities, such as the globally averaged flow quantities, but only depends on local quantities. This is a very desirable feature for prescribing the open boundary condition.

### 3.2 *Simplified Orlanski Method by Camerlengo and O'Brien* [3]

In this method, the local phase speed $c$ is evaluated according to Orlanski's method with the exception of the following fundamental differences: when the local phase speed is outward, a limiting outflow boundary condition is prescribed, and when the local phase speed is inward, an inflow boundary condition is prescribed:

$$\begin{aligned} \phi_k^{n+1} &= \phi_k^{n-1}, && \text{if} \quad c \leqslant 0 \quad \text{(inflow boundary condition)}, \\ &= \phi_{k-1}^{n}, && \text{if} \quad c > 0 \quad \text{(outflow boundary condition)}. \end{aligned} \tag{3.8}$$

Notice that the formulations of Camerlengo and O'Brien for inflow and outflow boundary conditions are not exactly the same as Eq. (3.8) since they used a staggered grid both in space and in time, although the basic concept of their formulation is described by Eq. (3.8). Their limited test results for Rossby and Kelvin waves show this method is better than the original Orlanski method. We believe, however, that further detailed tests on other types of problems should be carried out before any conclusion is drawn. Our preliminary test using Eq. (3.8) shows that Orlanski's original idea is superior for the problem presented here. A more detailed description of this test will be given in Section 5.

### 3.3 *The Present Method*

Orlanski's original finite-difference representation of Eq. (3.1) is a three-time-level explicit leapfrog method. His differencing is not used in the present method, simply because it requires three previous time levels (Eq. 3.3), and our marching scheme requires only one previous time level. For the method to be used here, a forward in time, upwind in space differencing scheme is applied to implement the radiation boundary condition. It is very simple and stable and has several useful numerical features for implementing an open boundary condition. The finite-difference form of the radiation condition becomes

$$(\phi_k^{n+1} - \phi_k^n)/\Delta t = -c[(\phi_k^n - \phi_{k-1}^n)/\Delta y]. \tag{3.9}$$

The phase speed $c$ is numerically evaluated at the closest interior point to the open boundary

$$c = -[(\phi_{k-1}^{n+1} - \phi_{k-1}^{n})/(\phi_{k-1}^{n} - \phi_{k-2}^{n})]\ (\Delta y/\Delta t); \tag{3.10}$$

and for the boundary point, we have

$$\phi_k^{n+1} = (1 - c(\Delta t/\Delta y))\phi_k^n + c(\Delta t/\Delta y)\phi_{k-1}^n. \tag{3.11}$$

Equation (3.11) is similar to Eq. (3.4) of the original Orlanski method. The boundary value $\phi_k^{n+1}$ is extrapolated from the values of $\phi$ near the boundary at the previous time step and is a function of phase speed $c$. The present method is basically a simple linear extrapolation in terms of the Courant number $c\,\Delta t/\Delta y$.

Like the original Orlanski method, the present formulation (3.11) gives the exact solution in the two limiting cases. When $c = \Delta y/\Delta t$,

$$\phi_k^{n+1} = \phi_{k-1}^n \qquad \text{(limiting outflow condition)},$$

and in the limit $c = 0$, Eq. (3.11) becomes

$$\phi_k^{n+1} = \phi_k^n \qquad \text{(limiting inflow condition)}.$$

The phase speed is limited by 0 and $\Delta y/\Delta t$; i.e., the same constraint, Eq. (3.7), is applied in the present method.

In the numerical integration scheme used in this study, Eq. (2.6), the boundary values of the first and second derivatives, as well as the boundary values themselves, are all required. Once all the values of interest are computed, including boundary values using Eq. (3.11) at the new time level $(n + 1)$, the first and second derivatives at the boundary can be directly obtained from the radiation condition Eq. (3.1), i.e.,

$$(\partial\phi/\partial t)^{n+1} = -c(\partial\phi/\partial y)^{n+1}, \qquad (\partial^2\phi/\partial t^2)^{n+1} = c^2(\partial^2\phi/\partial y^2)^{n+1}, \tag{3.12}$$

where $c$ is the phase speed evaluated from Eq. (3.10) for each variable.

Since each fluid dynamic variable is calculated separately using different differential governing equations, the corresponding phase speed $c$ is different for each variable and must also be evaluated separately. It is assumed that the phase speed of the pressure at the boundary also satisfies the radiation condition. It was previously mentioned that special attention is needed in prescribing pressure boundary conditions, and we may not evaluate the local phase speeds for the velocity and pressure independently. But to obtain a general and tractable relation between the velocity and the pressure at the boundary is beyond the scope of this study. In the present method an implicit differencing scheme is applied in order to retain numerical stability for the pressure boundary rather than the explicit scheme which is applied to all other variables of interest. Equations (3.10) and (3.11) for the pressure then become

$$c = [(P_{k-1}^{n+1} - P_{k-1}^{n})/(P_{k-1}^{n+1} - P_{k-2}^{n+1})]\ (\Delta y/\Delta t) \tag{3.13}$$

and

$$P_k^{n+1} = (P_k^n + (c\Delta t/\Delta y)\, P_{k-1}^{n+1})/(1 + (c\Delta t/\Delta y)). \tag{3.14}$$

Effects of this slight modification will be discussed in Section 5.

## 4. Validation Test Cases

Three linear problems are selected as test models for comparison. The main reason for choosing a linear problem is the availability of the exact solutions; hence, a direct comparison can be carried out. The first two test cases are unstratified flow problems, selected mainly for debugging of the computer code; the third case is a stratified flow. The latter problem is an ideal test case for investigation of the propagation of internal waves through a boundary. In order to understand the effectiveness of the open boundary condition, both calculations with an open boundary condition and a free-slip boundary condition are made using the same computational domain. The domain sizes used in the present test cases are significantly smaller than (as small as $\frac{1}{16}$ of) the domain sizes which we consider necessary to avoid boundary interactions with the free-slip boundary condition. All results are presented in a nondimensional form: length is nondimensionalized by a diameter $D$ and velocity by a speed $U_0$.

### 4.1 *Laminar Nonstratified Wake of a Towed Axisymmetric Body*

The axisymmetric laminar wake is an excellent test case for investigation of the effectiveness of the open boundary condition for a parabolic flow problem. The computed numerical solution can be directly compared with the self-similar solution for the axial velocity defect $u$,

$$\frac{u}{U_0} = \frac{C_D \,\mathrm{Re}}{16\pi} \frac{1}{\bar{x}} e^{-\mathrm{Re}\,\bar{r}^2/4\bar{x}}, \tag{4.1}$$

where $\bar{x} = x/D$, $\bar{r} = r/D$, and $D$ is the diameter of the towed slender body. We have also chosen the following set of parameters: $\mathrm{Re} = U_0 D/\nu = 100$, $C_D = 0.22$, initial station $\bar{x}_i = 6$, and final station $\bar{x}_f = 300$. The initial distribution for the axial velocity comes directly from Eq. (4.1); the horizontal and vertical velocities are obtained through an iterative scheme to satisfy the incompressibility condition. A full rectangular domain was used for the purpose of debugging, although only a quarter plane is necessary in this test case due to the axisymmetry of the flow. In earlier numerical experimentation, a computational domain with dimensions of $18.4\,D$ in both horizontal and vertical directions was selected as an optimum size for a free-slip boundary condition calculation. In the present test case, the domain size is reduced to $4.1\,D$ in both directions. The mesh is a strongly stretched variable mesh with $b_1 = b_2 = 0.2$ (refer to Appendix A). The minimum and maximum mesh sizes are $\Delta y_{\min} = \Delta z_{\min} = 0.1\,D$ at the center of the domain and $\Delta y_{\max} = \Delta z_{\max} = 0.825\,D$ at the far

boundaries with a total of 29 points in each direction. Notice that the domain size used here becomes smaller than the wake size at downstream stations. The reason for choosing such a small domain is to test the radiation condition by demonstrating that the wake boundary can pass through the open walls without any numerical distortion.

Figure 1 contains the comparison of the maximum axial velocity defect evaluated from the self-similar solution, Eq. (4.1), with the numerical result. Even with a very small domain, the numerical result shown by a solid line, obtained by using an open boundary condition, agrees very well with the exact solution which follows a $x^{-1}$ decay law. On the other hand, the numerical result using a free-slip boundary condition and the same computational mesh, shown by a dotted line in Fig. 1, shows a good agreement initially but begins to deviate from the exact solution after $\bar{x} = 150$. This indicates that the domain size is too small for the free-slip boundary condition calculation; as the wake boundary grows, it eventually exceeds the domain size.

The contour plots of axial velocity are shown in Fig. 2. It illustrates the wake growth in the downstream direction. Linearizing axial velocity equation (2.1), we have in cylindrical coordinates

$$U_0 \frac{\partial u}{\partial x} = \frac{v}{r} \frac{\partial}{\partial r} \left( r \frac{\partial u}{\partial r} \right), \tag{4.2}$$

which is the well-known heat diffusion equation. The contours of velocity $u$ (or

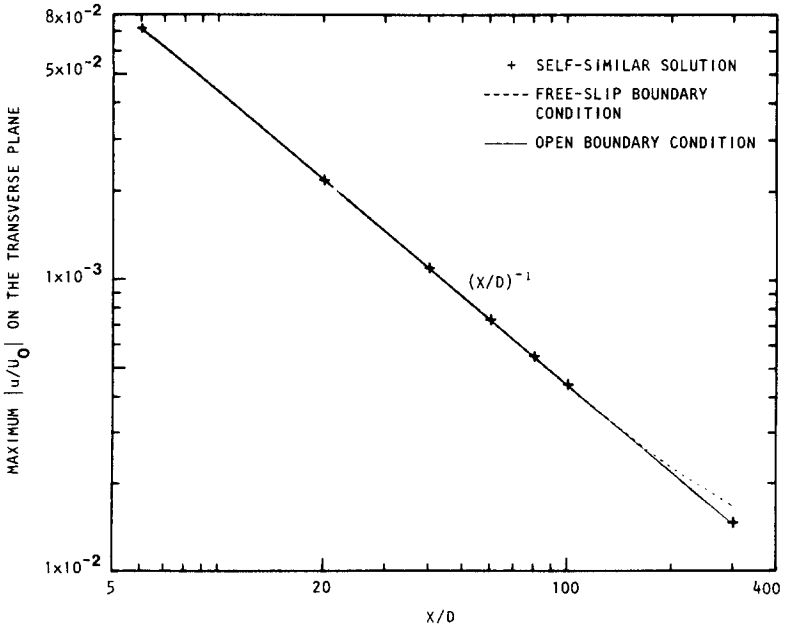


FIG. 1. Variation of the maximum axial velocity excess with downstream distance for the laminar nonstratified wake of a towed slender body.

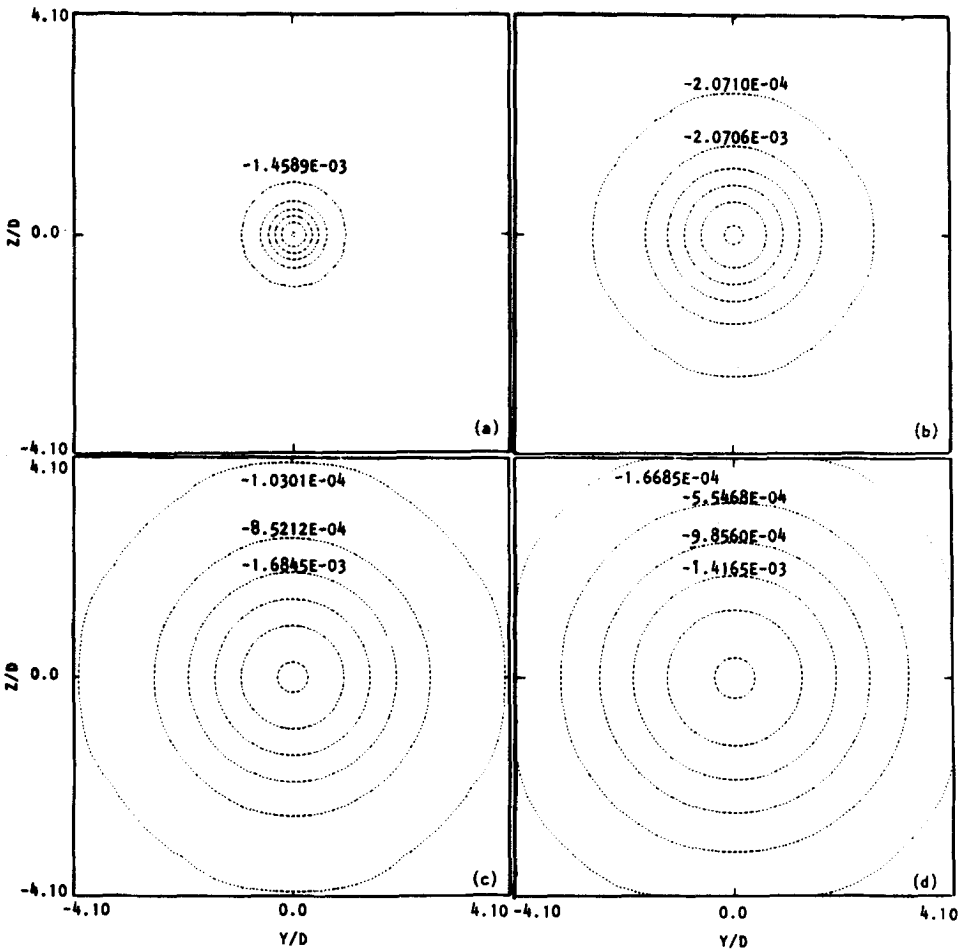


FIG. 2. Contour plots of the axial velocity excess with downstream distance: (a) $X/D = 6.0$, (b) $X/D = 42.6$, (c) $X/D = 105.1$, (d) $X/D = 192.6$.

isotherms) are circular and should grow through the open boundary without any distortion. As is seen, the present version of the open boundary condition performs well. The circular wake boundary passes through the computational boundaries without suffering any appreciable distortion.

### 4.2 *Laminar Nonstratified Wake of a Self-Propelled Axisymmetric Body*

This calculation is designed to validate the open boundary condition for an axisymmetric momentumless wake by comparison with the following self-similar solution,

$$\frac{u}{U_0} = (C/\bar{x}^2)(1 - (\eta^2/4))e^{-\eta^2/4}, \tag{4.3}$$

where

$$\eta = r\sqrt{U_0/vx}.$$

Due to the symmetry of the flow, the calculation is carried out on a quarter plane with a symmetry boundary condition applied on the left and bottom sides and the open boundary condition on the right and top sides of the domain. Previous numerical tests showed that the optimum domain size with a free-slip boundary condition on all sides is about 6.54 $D$ in both directions. In the present test case, the domain size is reduced to 3.28 $D$ in both vertical and horizontal directions, which produces about a factor of four reduction in the domain size. The mesh is also a strongly stretched variable mesh with $b_1 = b_2 = 0.173$ and 16 points in each direction.

Figure 3 contains the variation of maximum axial velocity versus the axial distance $\bar{x}$. Numerical solutions with open and free-slip boundaries are compared with the self-similar solution. As is demonstrated in the figure, perfect agreement is found for the open boundary case: the $x^{-2}$ decay law is strictly followed throughout the numerical calculation. The numerical solution using the free-slip boundary condition, however, starts to deviate approximately after $\bar{x} = 100$, and it decays faster than the exact solution.

Based on these limited test results for parabolic-type flows, we may conclude that the newly devised open boundary condition performs very well even with a small

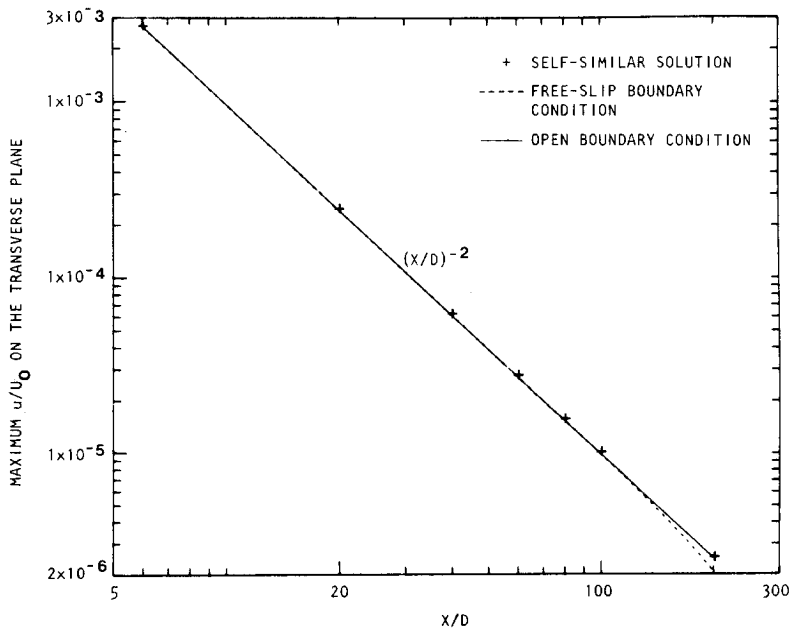


FIG. 3. Variation of the Maximum axial velocity excess with downstream distance for the laminar nonstratified wake of a self-propelled body.

computational domain. In the next section, we shall discuss the performance of the open boundary condition for density stratified flows which are hyperbolic in nature.

### 4.3 *Collapse of a Well-Mixed Region in a Linearly Stratified Fluid*

The internal wave field generated by the collapse of a well-mixed region in an incompressible and stratified fluid has been studied extensively in recent years. A theoretical analysis has been conducted by Hartman and Lewis [6] for a partially mixed cylindrical region. Following the same approach, the closed-form solution for the internal wave field generated by a density perturbation has been derived and is discussed in Appendix B.

Given the following initial distribution of the deviation of the density from its ambient state $\rho_0$,

$$\rho' = \varepsilon r \sin\theta e^{-(r/r_0)^2}, \tag{4.4}$$

where $\theta$ is the polar angle measured from the horizontal and $r_0$ is a characteristic length related to the diameter $D$ of the mixed region, the closed-form solution is

$$\begin{aligned}\frac{\rho'(r,\theta,t)}{\rho_0} = \frac{\varepsilon}{\rho_0}\frac{r_0^2}{r}\Bigg\{\frac{2}{Nt}\frac{r}{r_0}\sin\theta \sum_{l=0}^{\infty}(2l+1) \\ \times \frac{\Gamma(l+2)}{\Gamma(2l+2)}\left(\frac{r}{r_0}\right)^{2l+1}\frac{\sin[(2l+1)\theta]}{\sin\theta} \\ \times J_{2l+1}(Nt)M\left[l+2, 2l+2, -\left(\frac{r}{r_0}\right)^2\right]\Bigg\},\end{aligned} \tag{4.5}$$

where $N$ is the Brunt–Väisälä frequency, $J$ represents the Bessel function of the first kind, and $\Gamma$ and $M$ represent the gamma function and the confluent hypergeometric function, respectively. For the fully mixed region considered here, we have $\varepsilon = -d\rho_0/dz$. The input parameters are $r_0/D = 0.346$, $\varepsilon r_0/\rho_0 = 3.12 \times 10^{-3}$. The quarter plane symmetry of the flow is utilized by centering the initial disturbance at the lower left-hand corner of the computational domain so that only one quadrant of the flow field needs to be computed. Previous numerical experimentation with free-slip boundary conditions on all sides showed that a computational domain with dimensions of $20\,D$ in both the horizontal and vertical directions is sufficiently large to minimize effects of reflection from the boundary. Computational domains for the test cases to be discussed here range from $5\,D$ to $10\,D$. The mesh is again a strongly stretched variable mesh with $b_1 = b_2 = 0.10845$, and $\Delta y_{\min} = \Delta z_{\min} = 0.15\,D$ at the lower left-hand corner, and $\Delta y_{\max} = \Delta z_{\max} = 1.134\,D$ at the far boundaries. A total of 27 points in each direction for the $10\,D$ case and 21 points for the $5\,D$ case are used.

Results of numerical calculations using both the open and free-slip boundary condition are compared directly with the exact solution in Figs. 4–6 up to 10 Brunt–Väisälä periods. Isopycnic displacements, which are defined as $\zeta = -\rho'/(d\rho_0/dz)$, are evaluated from the closed-form solution, Eq. (4.5), and presented together with the

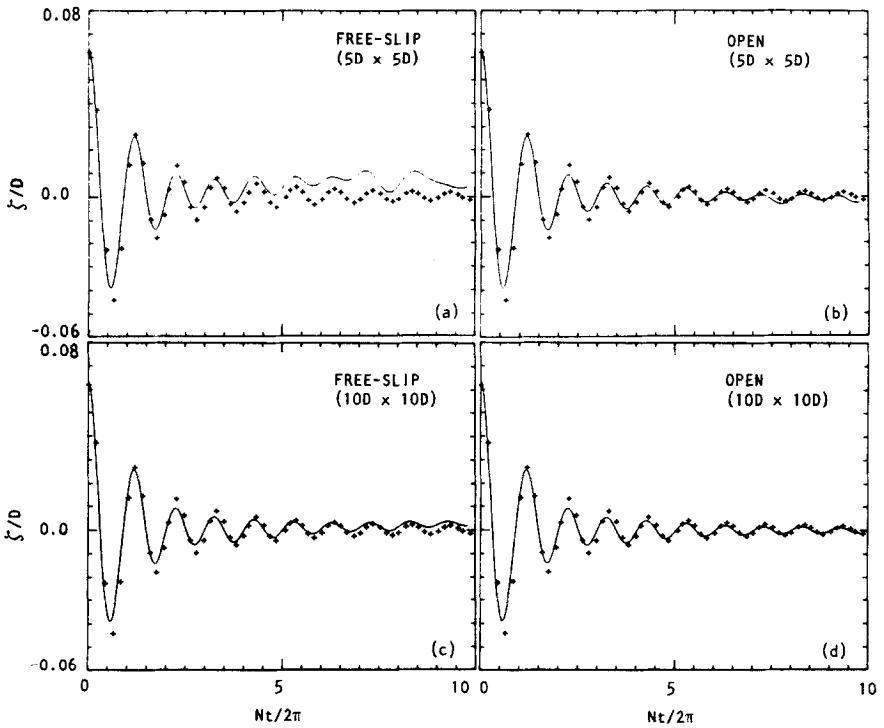


FIG. 4. Variation of isopycnic displacement with time in Brunt–Väisälä periods for collapse of a well-mixed region. The probe location is (0 $D$, 0.5 $D$) on the transverse plane: (—) numerical results, (+) exact linear solution (Eq. (4.5)).

numerical solutions. The performance of the open boundary condition is remarkably good. After the initial collapse, the envelopes of the displacement show a $(Nt)^{-3/2}$ asymptotic behavior. This clearly shows that the fully mixed region collapse problem falls well within the realm of the linear approximation. It also demonstrates that, with a smaller computational domain, the third-order marching scheme using the open boundary condition can accurately compute the internal wave field generated by a collapsing wake.

A time history of the potential and kinetic energy per unit length on the transverse plane are shown in Figs. 7 and 8. It can be shown [4] that the potential energy in a stratified fluid with constant $d\rho_0/dz$ is given by

$$\text{P.E.} = \frac{-g}{2(d\rho_0/dz)} \iint (\rho')^2 \, dy \, dz, \tag{4.6}$$

and kinetic energy is

$$\text{K.E.} = \tfrac{1}{2} \iint \rho(v^2 + w^2) \, dy \, dz, \tag{4.7}$$

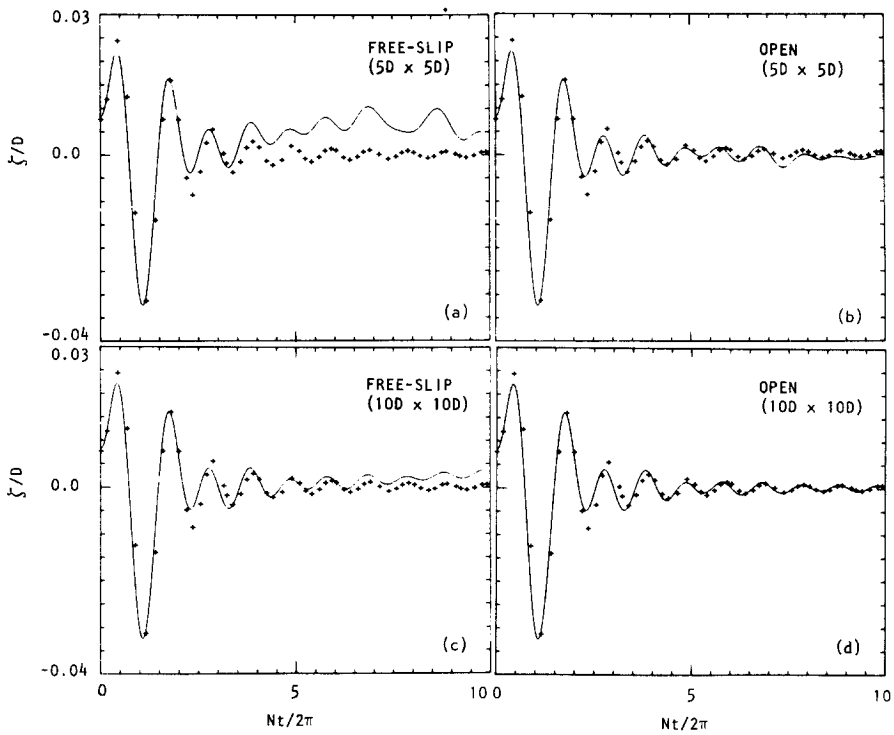


FIG. 5. Variation of isopycnic displacement with time in Brunt–Väisälä periods for collapse of a well-mixed region. The probe location is (0.5 $D$, 0.5 $D$) on the transverse plane: (—) numerical result; (+) exact linear solution (Eq. (4.5)).

where $\rho = \rho_0 + \rho'$. Due to the very slow convergence of the series solution of Eq. (4.5) and the difficulty of integrating $(\rho')^2$ from this equation analytically, it is not feasible to compare the exact solution for the potential and kinetic energy with the numerical solution. These figures, however, reveal interesting features of the open boundary conditions versus the free-slip boundary condition. After the initial peak, the mean kinetic energy level decreases both for free-slip and open boundary conditions. This is considered to be a result of truncation error and the lack of summability of the numerical scheme. The kinetic energy of the open boundary case, shown in solid line, decreases faster than that of the solid boundary condition. This is expected since a portion of the kinetic energy for the open boundary case leaves the system as a result of the outward propagation of internal waves through the boundary. After the initial collapse, potential energy for the open boundary condition, indicated by the solid line in Fig. 7, stays at a nearly constant mean level up to 6 Brunt–Väisälä periods. The irregular oscillations after 6 Brunt–Väisälä periods are probably due to wave reflection at the open boundary. We must realize that no

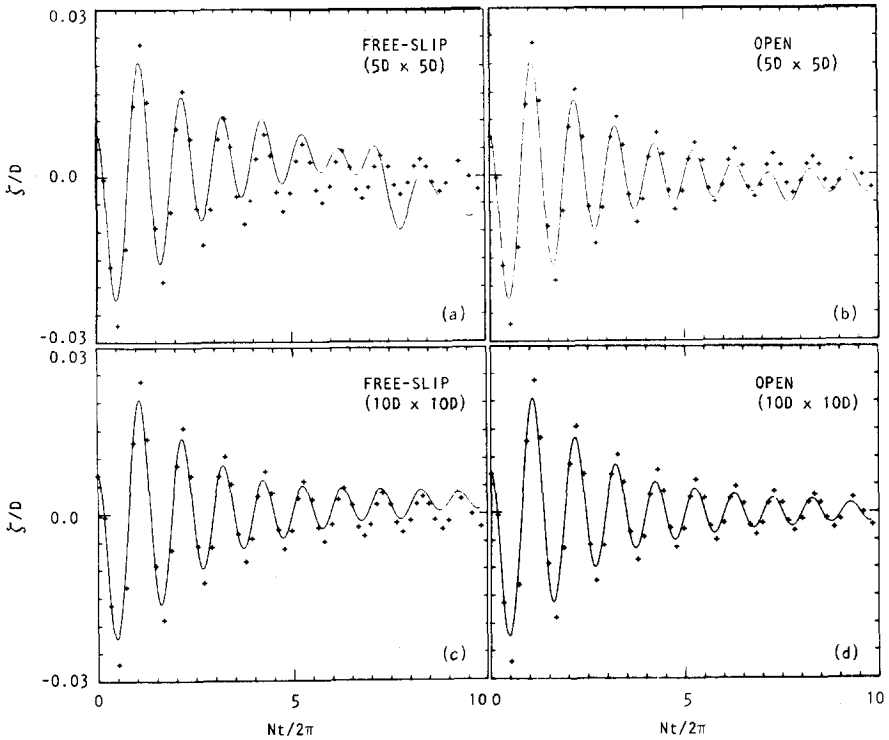


FIG. 6. Variation of isopycnic displacement with time in Brunt–Väisälä periods for collapse of a well-mixed region. The probe location is (0 $D$, 0.75 $D$) on the transverse plane: (—) numerical result; (+) exact linear solution (Eq. (4.5)).

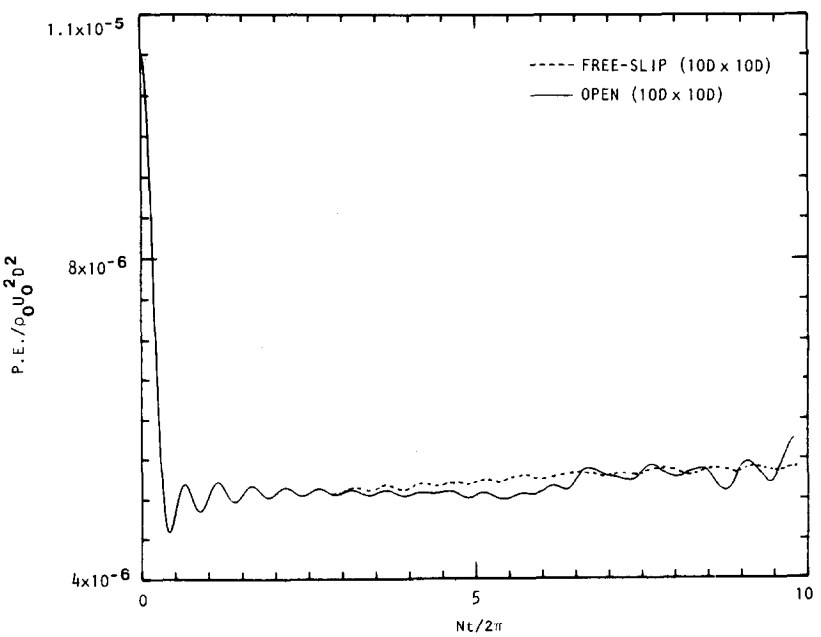


FIG. 7. Variation of potential energy per unit length with time in Brunt–Väisälä periods for collapse of a well-mixed region.

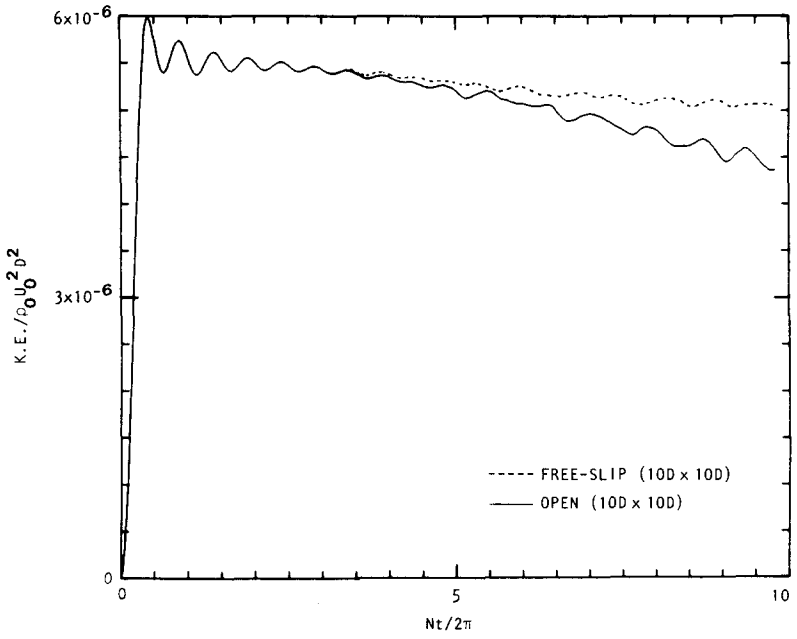


FIG. 8. Variation of kinetic energy per unit length with time in Brunt–Väisälä periods for collapse of a well-mixed region.

radiation boundary condition is completely free from wave reflections for all general problems. The potential energy for the free-slip boundary case starts to deviate from the constant mean level somewhat earlier (about 3 B.V. periods) than for the open boundary case due to the stronger reflections at the boundary.

## 5. Discussion and Recommendations

A Sommerfeld radiation condition is used to prescribe an open boundary condition. The phase speed is evaluated numerically at the closest interior point to the

order scheme, forward in time and upwind in space, has been employed.

As mentioned before, preliminary tests using Camerlengo and O'Brien's method, Eq. (3.8), have been conducted for the collapse of a well-mixed region in a linearly stratified fluid using a domain size $5D \times 5D$. Figure 9 shows the variation of the isopycnic displacement with time in Brunt–Väisälä periods at three locations (0, 0.5 $D$), (0.5 $D$, 0.5 $D$), and (0, 0.75 $D$). These results can be directly compared with the results shown in Figs. 4a and b, 5a and b, and 6a and b. The unacceptable reflection at the boundaries can easily be observed. The boundary condition, like

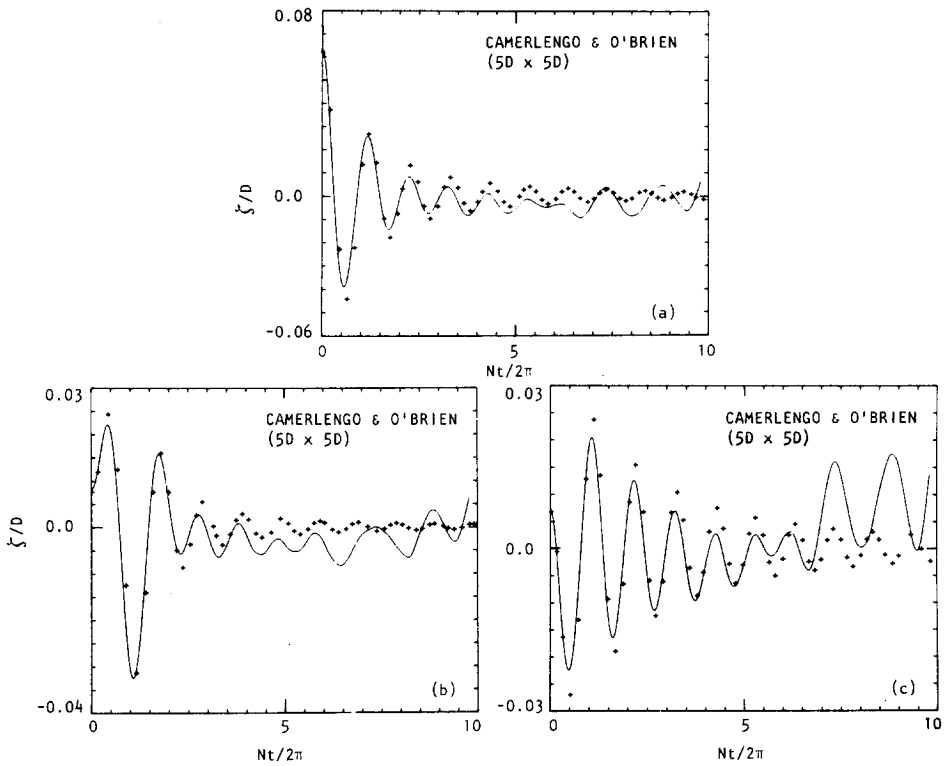


FIG. 9. Variation of isopycnic displacement with time in Brunt–Väilälä periods for collapse of a well-mixed region. The probe locations are: (a) (0 $D$, 0.5 $D$), (b) (0.5 $D$, 0.5 $D$), and (c) (0 $D$, 0.75 $D$): (—), numerical result using a simplified open boundary condition according to Camerlengo and O'Brien; (+) exact linear solution (Eq. (4.5)).

Eq. (3.8), should perform well if the numerical solution is characterized by a monochromatic wave with phase speed approximating $\Delta y/\Delta t$. If, however, it is not the case, i.e., $0 < c < \Delta y/\Delta t$, reflections will occur at the boundaries. We believe that Camerlengo and O'Brien's method can be regarded as a zeroth-order approximation to the radiation boundary condition, as opposed to our first-order method, Eq. (3.11).

Again, we emphasize that special care is needed for implementing the open boundary condition if the velocity and density are solved directly as primitive variables, and if the pressure is obtained from a Poisson equation. All numerical methods solving primitive variables require both velocity and pressure boundary conditions. If the explicit forward in time and upwind in space differencing scheme of Eq. (3.11) is applied for all the variables of interest including the pressure, then the boundary condition becomes unstable. More numerical experimentation has revealed that the numerical solution is very sensitive to the methodology employed for the pressure boundary condition. This is probably a result of the strong coupling between

the velocity and pressure fields. Clearly, the phase speeds for the velocity and pressure near the boundary should not be independently specified. This, however, is beyond the scope of our study here. Instead, in order to retain numerical stability, an implicit differencing scheme, Eq. (3.14), is applied for the pressure boundary condition. We also found that if the Neuman boundary condition ($\partial\phi/\partial\eta = 0$) for the pressure equation is used, results for all the test cases are very poor. The reason for this is that the Neuman boundary condition for the pressure equation is incompatible with the radiation boundary condition for all the other variables. Based on these limited test results, the implicit pressure boundary condition is the most preferred choice so far for implementing the radiation boundary condition. Further improvement of the pressure boundary condition should be pursued in the future.

## 6. Conclusion

The objective of this study was to carry out a rigorous evaluation of the performance of a modified Orlanski open boundary condition. The proposed open boundary condition is based on a phase speed calculated locally. Such a local treatment seems to allow waves to propagate through the open boundaries. Three linear model problems are used to quantify the accuracy of the radiation condition. The limited test results show the proposed open boundary condition performs very well for both parabolic and hyperbolic problems. It is demonstrated that the proposed open boundary condition is definitely better than the free-slip boundary condition. Consequently, we can reduce the computing cost by about 50 percent through the reduction of the computational domain size while still maintaining the same order of accuracy. Some wave reflections near the boundary are inevitable, however, since there is no perfect open boundary condition for a wide variety of flow problems. Although the domain size can be reduced significantly by using the open boundary condition, special attention is still needed when determining the size of the computational domain.

## APPENDIX A: Construction of a Variable Mesh

When solving a finite-difference equation on a variable mesh, one commonly encountered problem is that unrealistic wave reflection or loss of information occurs if the variable mesh scheme is not properly chosen for the physical problem. Problems normally arise when excessive stretching of the mesh is employed. An ideal variable mesh is the one which employs a minimal number of mesh points in the inactive region of the wake flow without distorting the solution in the active region. To find this ideal mesh for the wake flow problem, a simplified analysis based upon the radiation condition

$$\partial f/\partial t + c(\partial f/\partial y) = 0, \tag{A.1}$$

which represents internal wave propagation, is sufficient. Assume a coordinate transformation of the form $y = y(y')$ so that Eq. (A.1) can be solved by a finite-difference method on the $y'$-plane on a uniform mesh. Furthermore, Fourier analyzing $f$ into $\hat{f}(y')e^{j\omega t}$ and finite differencing the equation, one has

$$j\omega\hat{f}_i + c\frac{dy'}{dy}\frac{\hat{f}_{i+1} - \hat{f}_{i-1}}{2\Delta y'} = 0.$$

Let $\hat{f}_i = \hat{f}_0 e^{ji\theta}$ and rearrange to give

$$|\sin\theta| = \left|\frac{\omega}{c}\Delta y'\frac{dy}{dy'}\right|. \tag{A.2}$$

The requirement that the left-hand side should always be less than one imposes a constraint on the magnitude of the stretching function $dy/dy'$. Consider $y'$ equal to the index $i$ so that $\Delta y' \equiv 1$ and $dy/dy' = \Delta y(i)$; then the above equation simply states that

$$\omega\Delta y(i) < c \tag{A.3}$$

or the longest wavelength included should not propagate faster than the wave phase speed $c$. This criterion should determine the type and degree of stretching to be imposed.

Consider the two-dimensional ($y, z$ plane) steady propagation of internal waves. From the dispersion relation

$$\omega = N(k_y/(k_y^2 + k_z^2)^{1/2})$$

for $k_z \equiv 0$ (horizontally propagating waves), one has $c = \omega/k_y = N/k_y$, where $N$ is the Brunt–Väisälä frequency. Rewriting Eq. (A.3) in terms of $k_y$, one has

$$k_y\Delta y(i) < 1$$

or

$$\Delta y(i) < y/Nt$$

for all indices $i$, where $t$ represents time. The limiting case is then

$$dy/di \cong y/Nt. \tag{A.4}$$

This is the fundamental relation for the ideal variable mesh for the case of stratified wake flow. We have chosen to expand the mesh somewhat more slowly than the limiting case solution would allow, using the relation

$$y = \text{YZERO} + a\sinh[i - \text{ICEN})b_1]. \tag{A.5}$$

Here, YZERO is the distance from the wake center to the closest cell center, ICEN is the $y$-index of the cell containing the wake center, and $b_1$ is a stretching factor which should optimally be chosen to be less then $1/Nt$. In practice, a value for $b_1$ of approximately 0.1 has been found to provide adequate resolution for a stratified flow calculation, whereas, for a nonstratified calculation, a slightly larger value on the order of 0.2 may be used.

The mesh spacing is determined by differentiating Eq. (A.5) with respect to the index $i$ to give

$$\Delta y(i) = ab_1 \cosh[(i - \text{ICEN})b_1]. \tag{A.6}$$

Equations (A.5) and (A.6) can then be solved to determine the constants $a$, $b_1$, IMAX, YMAX $= y$(IMAX), and $\Delta y$(ICEN). Similarly, we have

$$\Delta z(j) = ab_2 \cosh[(j - \text{JCEN})b_2]$$

for the vertical coordinate $z$.

## APPENDIX B
## The Closed-Form Solution for the Internal Wave Field Generated by a Density Perturbation

Consider two-dimensional motion in an unbounded, inviscid, incompressible, and linearly stratified fluid. The linearized Boussinesq equations of motion governing $v$ and $w$, the velocities, $\psi$, the stream function, and $\rho'$, the deviation of the density from its ambient state $\rho_0$ in which the fluid is at rest are

$$v = \partial\psi/\partial z, \qquad w = -\partial\psi/\partial y, \tag{B.1}$$

$$\frac{\partial \rho'}{\partial t} - \frac{\partial \psi}{\partial y}\frac{d\rho_0}{dz} = 0, \tag{B.2}$$

$$\frac{\partial^2}{\partial t^2}\nabla^2\psi + N^2\frac{\partial^2 \psi}{\partial y^2} = 0, \tag{B.3}$$

where $y$ and $z$ are the horizontal and vertical directions, respectively. Here

$$N^2 = -(g/\rho_0)(d\rho_0/dz)$$

is the Brunt–Väisälä frequency, and $g$ is the gravitational acceleration along the negative $z$-axis.

The exact solution of Eq. (B.3) for the initial conditions corresponding to a partially mixed cylindrical wake has been obtained by Hartman and Lewis [6] using

Fourier analysis. Their results can be generalized; letting $f$ be either $\rho'$ or $\psi$, the solution of Eq. (B.3) for the arbitrary initial conditions $f(y, z, 0)$ and $\partial f/\partial t|_{t=0}$ is

$$f(y,z,t)=\frac{1}{4\pi^2}\int_{-\infty}^{\infty}\int_{-\infty}^{\infty}\frac{1}{2}\left[F_1(k_y,k_z)\pm\frac{F_2(k_y,k_z)}{i\omega}\right]e^{i(k_y y+k_z z\pm\omega t)}\,dk_y\,dk_z, \tag{B.4}$$

in which

$$\omega = Nk_y(k_y^2+k_z^2)^{-1/2}, \tag{B.5}$$

$$F_1(k_y,k_z)=\int_{-\infty}^{\infty}\int_{-\infty}^{\infty}f(y,z,0)\,e^{i(k_y y+k_z z)}\,dy\,dz, \tag{B.6}$$

$$F_2(k_y,k_z)=\int_{-\infty}^{\infty}\int_{-\infty}^{\infty}\left.\frac{\partial f}{\partial t}\right|_{t=0}e^{-i(k_y y+k_z z)}\,dy\,dz, \tag{B.7}$$

and the results of the integrals in Eq. (B.4) for each sign should be superposed.

In the present study, a smoothed version of the initial density perturbation is used to remove the discontinuity. The initial conditions are

$$\rho' = \varepsilon r\sin(\theta+\alpha)e^{-(r/r_0)^2}, \qquad (\partial\rho'/\partial t)|_{t=0}=0, \tag{B.8}$$

where $\theta$ is the polar angle measured from the horizontal, $\alpha$ is a tilt angle measured from the vertical, and $r_0$ is a characteristic length related to the radius of the mixed region. For the perturbed density field, the exact solution of Eq. (B.3) with initial conditions (B.8) is found to be

$$\frac{\rho'(\mathbf{x},t)}{\rho_0}=\frac{\varepsilon r_0^4}{8\rho_0}\left\{z\cos\alpha\int_0^{\infty}k^3e^{-(kr_0)^2/4}\left[\frac{J_1(L^+)}{L^+}+\frac{J_1(L^-)}{L^-}\right]dk\right.$$
$$\left.+\sin\alpha\int_0^{\infty}k^2e^{-(kr_0)^2/4}\left[(ky+Nt)\frac{J_1(L^+)}{L^+}-(ky-Nt)\frac{J_1(L^-)}{L^-}\right]dk\right\}, \tag{B.9}$$

where

$$L^{\pm}=\sqrt{(ky\pm Nt)^2+(kz)^2}, \qquad k=\sqrt{k_y^2+k_z^2},$$

and $J_1$ is the first-order Bessel function of the first kind. Expression (B.9) is evaluated by first observing that

$$\frac{J_1(L^+)}{L^+}+\frac{J_1(L^-)}{L^-}=\frac{4}{Ntkr}\sum_{l=0}^{\infty}(2l+1)J_{2l+1}(Nt)J_{2l+1}(kr)\frac{\sin[(2l+1)\theta]}{\sin\theta} \tag{B.10}$$

and

Substituting (B.10) and (B.11) into (B.9) and evaluating the resulting integrals, we obtain

$$\frac{\rho'(r,\theta,t)}{\rho_0} = \frac{\varepsilon}{\rho_0}\frac{r_0^2}{r}\left\{-\sin\alpha \sum_{l=1}^{\infty} 2l \frac{\Gamma(l+1)}{\Gamma(2l+1)}\left(\frac{r}{r_0}\right)^{2l}\frac{\sin(2l\theta)}{\sin\theta}\right.$$
$$\times J_{2l}(Nt)M[l+1, 2l+1, -(r/r_0)^2]$$
$$+\frac{2}{Nt}\frac{r}{r_0}\sin(\theta+\alpha)\sum_{l=0}^{\infty}(2l+1)\frac{\Gamma(l+2)}{\Gamma(2l+2)}\left(\frac{r}{r_0}\right)^{2l+1}$$
$$\left.\times\frac{\sin[(2l+1)\theta]}{\sin\theta}J_{2l+1}(Nt)M\left[l+2, 2l+2, -\left(\frac{r}{r_0}\right)^2\right]\right\}, \quad \text{(B.12)}$$

where $M$ represents the confluent hypergeometric function. The closed-form solution (B.12) is a continuous function for all $r$ and $\theta$.

## Acknowledgment

This work was performed under the technical supervision of the Applied Physics Laboratory at Johns Hopkins University. The authors wish to acknowledge the support and many helpful suggestions from Dr. Michael Roth at APL/JHU.

## References

1. I. Orlanski, *J. Comput. Phys.* **21** (1976), 251.
2. R. K. C. Chan, *in* "Second International Conference on Numerical Ship Hydrodynamics," (J. V. Wehausen and N. Salvesen, Eds.), pp. 39–52, University Extension Publications, Univ. of California at Berkeley, 1977.
3. A. L. Camerlengo and J. J. O'Brien, *J. Comput. Phys.* **35** (1980), 12.
4. R. K. C. Chan, *J. Comput. Phys.* **22** (1976), 74.
5. F. H. Harlow and J. E. Welch, *Phys. Fluids* **8** (1965), 2182.
6. R. J. Hartman and H. W. Lewis, *J. Fluid Mech.* **51** (1972), 613.